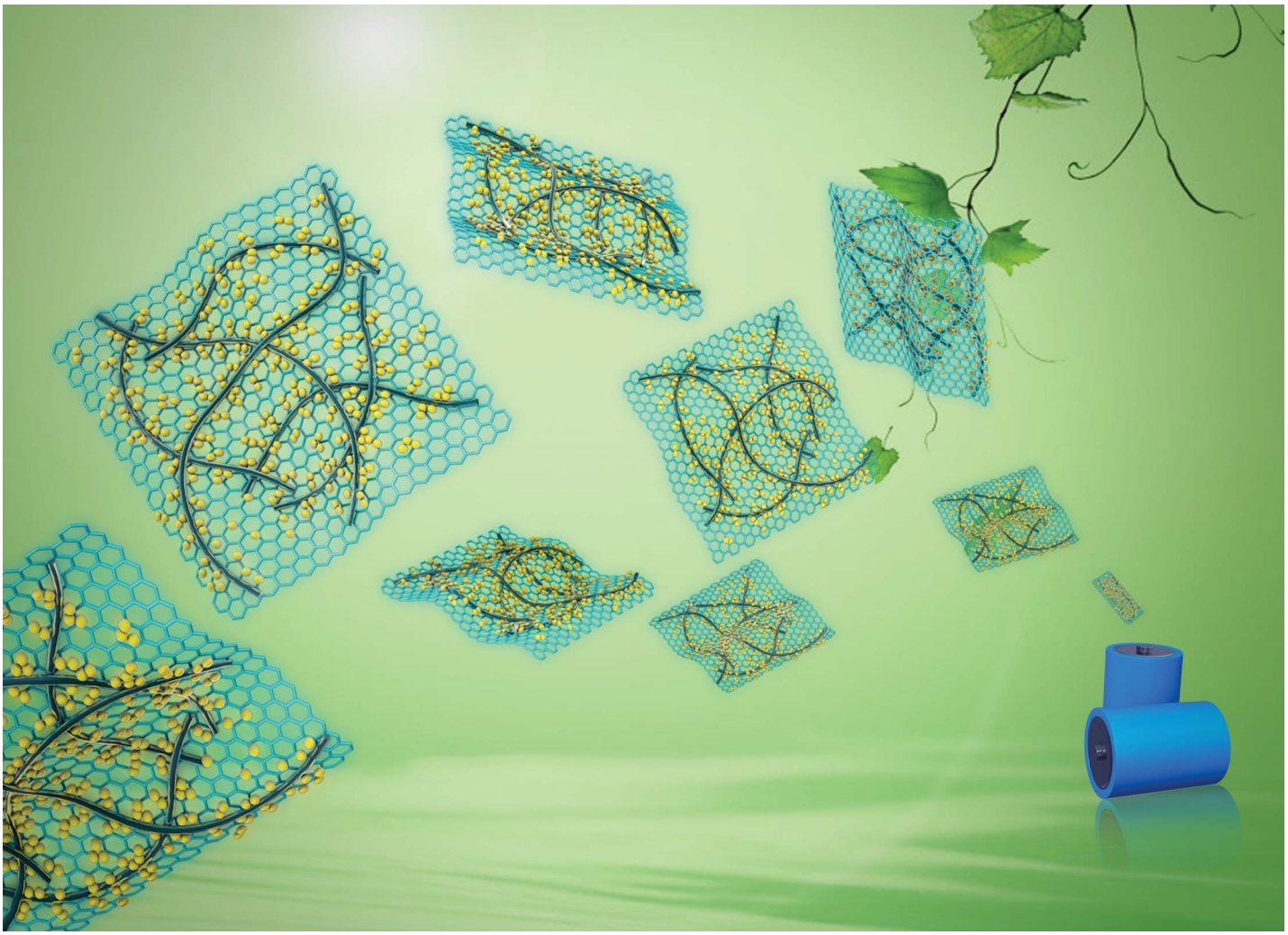

Showcasing the work on carbon nanotube/graphene hybrid materials as sulfur hosts for cathodes of lithium–sulfur batteries presented by Dr. Li Sun, Prof. Jiaping Wang, Prof. Shoushan Fan, and co-workers, Department of Physics and Tsinghua-Foxconn Nanotechnology Research Center, Tsinghua University.

Title: Super-aligned carbon nanotube/graphene hybrid materials as a framework for sulfur cathodes in high performance lithium sulfur batteries

A binder-free sulfur/carbon nanotube/graphene composite electrode is fabricated by a scalable and facile ultrasonication-assisted method. Taking advantage of carbon nanotube/graphene hybrid materials as conducting framework, structural supports, and physical barriers, the sulfur composite electrode demonstrates high capacities, good reversibility, and excellent high-rate capability.

As featured in:

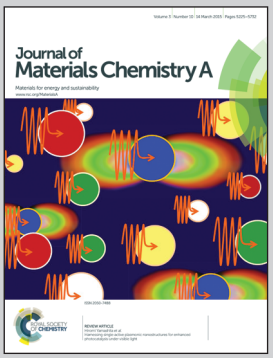

See Jiaping Wang *et al.*, *J. Mater. Chem. A*, 2015, **3**, 5305.

ROYAL SOCIETY OF CHEMISTRY

www.rsc.org/MaterialsA

Registered charity number: 207890

Journal of Materials Chemistry A

PAPER

View Article Online
View Journal | View Issue

Cite this: J. Mater. Chem. A, 2015, 3, 5305

Super-aligned carbon nanotube/graphene hybrid materials as a framework for sulfur cathodes in high performance lithium sulfur batteries†

Li Sun,[a] Weibang Kong,[a] Ying Jiang,[a] Hengcai Wu,[a] Kaili Jiang,[ab] Jiaping Wang*[ab] and Shoushan Fan[a]

Received 18th November 2014
Accepted 10th December 2014

DOI: 10.1039/c4ta06255h

www.rsc.org/MaterialsA

We report the use of super-aligned carbon nanotube/graphene (CNT/G) hybrid materials as a 3D conducting framework for sulfur accommodation. The CNT network acts as a skeleton to form a self-sustained cathode that is binder-free, highly conductive, and flexible. Graphene with a 2D sheet structure extends in an additional dimension to provide improved restriction for sulfur/polysulfides. Moreover, the CNT/G hybrid framework enables better dispersion of sulfur and allows each sulfur particle to closely attach to the conductive components, which greatly enhance the electronic conductivity and thereby approach the full potential of the active materials. With an optimized CNT/G ratio in the framework, the S–CNT/G nanocomposite exerts improved mechanical performance and favorable electrochemical characteristics compared to the S–CNT composite. Based on its superior structure, the S–CNT/G nanocomposite achieves a high discharge capacity of 1048 mA h g^{-1} at 1 C with a capacity fade as low as 0.041% per cycle over 1000 charge–discharge cycles. Excellent high-rate and long-term cycling performances are also revealed. These results demonstrate the great potential of the S–CNT/G nanocomposite as a flexible and binder-free cathode for Li–S batteries.

Introduction

Lithium sulfur batteries, with unparalleled theoretical capacity and other advantages including abundance of the raw material, low cost, and environmental benignity, have drawn an increasing amount of interest due to their potential for applications in next-generation high energy power systems.[1–4] Lithium (Li) and sulfur (S), with theoretical capacities of 3861 and 1672 mA h g^{-1} individually, can produce large gravimetric and volumetric energy densities of 2500 W h kg^{-1} and 2800 W h L^{-1}, respectively, assuming a complete reaction of lithium and sulfur to Li_2S. Despite the appealing theoretical characteristics, the practical application of Li–S batteries is restricted by the poor electrochemical performance of sulfur. Several shortcomings of the sulfur cathode, including the low ionic and electronic conductivities of sulfur and its various discharge products (Li_2S_x, x = 1–8), the high volume change of sulfur during lithiation, the dissolution of intermediate polysulfides into the electrolyte, and the so-called "shuttle effect", lead to low sulfur utilization and poor reversibility, which make sulfur not suitable for direct use as a cathode material for Li–S batteries. To solve these problems, composite electrodes are constructed by combining sulfur with conductive materials, of which carbon materials with high conductivity and abundant porosity (carbon nanotubes (CNTs),[5–10] graphene nanosheets,[11–17] porous carbon,[18–23] *etc.*) are considered as ideal sulfur hosts.

Among various nanostructured carbon materials, graphene and CNTs are extensively studied due to their excellent electrical conductivity, high surface area, mechanical durability, and the potential to form flexible and porous electrode structures.[24–27] Much work has been done by using graphene or CNTs as sulfur hosts to form cathodes for Li–S batteries, achieving significantly enhanced capacity, cycle stability, and rate capability. By incorporating sulfur into CNTs or graphene structures, the insulating sulfur particles are not only well connected electrically, but also effectively restricted by the continuous framework, significantly enhancing the sulfur utilization and the overall cycle performance. Besides, adsorption sites provided by the continuous framework formed by 1D CNTs or 2D graphene can also prevent the dissolution and shuttle of intermediate polysulfides to a certain extent, so that stable cycling and high efficiency can be maintained in Li–S batteries. However, CNTs or graphene materials with single dimension tend to agglomerate due to van der Waals interactions and large surface area, which limits their efficiency as sulfur hosts. Recently, hierarchical structures with CNTs effectively bonded with graphene have been developed to alleviate the self-aggregation and re-stacking of individual materials and also exert advantages of

[a]Department of Physics and Tsinghua-Foxconn Nanotechnology Research Center, Tsinghua University, Beijing 100084, China. E-mail: jpwang@tsinghua.edu.cn
[b]Collaborative Innovation Center of Quantum Matter, Beijing 100084, China

† Electronic supplementary information (ESI) available. See DOI: 10.1039/c4ta06255h

both components.[28] Typical CNT/G hybrid structures include single-walled CNT/G hybrids,[29] nitrogen-doped aligned CNT/G sandwiches,[28] MWCNT web/reduced graphene oxide nanostructures,[30] *etc.* Though improved electrochemical performance has been demonstrated in these hybrid structures compared to CNT-based or graphene-based ones, complex fabrication processes, such as catalytic growth or surface modification, are generally involved. Besides, the complex structures of CNT/G hybrids may set a limit to the incorporating method of the active material, which restrains the design flexibility of sulfur cathodes. In order to overcome these shortcomings, a more simple method to combine CNT and graphene into a hybrid framework and to fabricate a sulfur–CNT/G composite is needed. Based on these considerations, super-aligned CNTs (SACNTs) with large aspect ratio (>10^4), clean surface, and strong van der Waals force among tubes[31,32] are a good choice to serve as skeleton materials to combine with graphene and to form flexible and binder-free electrodes. A previous study has been reported by our group to synthesize binder-free nano S–SACNT composites by dissolving sulfur in one polar solvent and precipitating from it upon adding another polar solvent.[33] The precipitated sulfur nanoparticles deposit onto well dispersed SACNTs in the solvent and a binder-free composite can be formed after removing the solvent. High flexibility, excellent cycling performance, and impressive rate capability are achieved in the obtained nano S–SACNT composite. However, strict control on the experimental procedure, especially the speed of addition and position of the polar solvent, is required to ensure the homogeneity of the final product, which limits its application on a large scale.

Herein, based on SACNTs, we introduce a simplified ultrasonication-assisted method to fabricate flexible and binder-free sulfur–CNT/graphene (S–CNT/G) nanocomposites that exhibit superior long-term cycling stability and high-rate performances. Commercially obtained graphene is introduced as a 2D supplement to the 1D SACNTs, constructing a 3D hierarchical CNT/G conductive framework and physical barriers to constrain sulfur and its lithiation products. By dispersion of sulfur particles into graphene and SACNTs *via* intensive ultrasonication in water–ethanol mixed solution and subsequent removal of the solvent, flexible and binder-free S–CNT/G nanocomposites can be easily obtained. In the composite structure, SACNTs along with graphene provide a 3D conductive framework to facilitate electron transport, large porosity to accommodate the volume expansion of sulfur, and abundant adsorption points to immobilize sulfur and its lithiation products. Meanwhile, well-distributed sulfur nanoparticles avoid the bundling of SACNTs and the re-stacking of graphene, ensuring a more efficient 3D extended conductive network. The synergetic effect among graphene, SACNTs, and sulfur brings out enhanced electrochemical performance in the composite electrode, especially its high-rate capability and long-term cycle stability.

Experimental section

Material preparation

SACNT arrays with a diameter of 20–30 nm and a height of 300 μm were synthesized on silicon wafers by chemical vapor deposition (CVD), with iron as the catalyst and acetylene as the precursor. Details of the synthesis procedure can be found in previous papers.[31,32]

The S–CNT/G composite electrode was prepared as follows: sulfur powder (Beijing Dk Nano technology Co., Ltd.), SACNTs, and graphene (Nanjing XFNANO Materials Tech Co., Ltd) were simultaneously suspended in water–ethanol mixed solution with a water–ethanol ratio of 3 : 1. The mixture was intensively ultrasonicated using an ultrasonication probe (1000 W) for 30 min to form a uniform suspension. The resulting mixture was then dried at 50 °C to remove the solvent and a binder-free S–CNT/G nanocomposite was detached from the container. The sulfur loading was 50 wt% in the raw materials, and composites with different CNT/G ratios of 2 : 1, 1 : 1, and 1 : 2 were prepared. For comparison, a S–CNT (50 wt% S) composite was prepared following the same procedure as that of S–CNT/G composite, but without the addition of graphene.

Material analysis

The crystalline structures of SACNT, graphene, and S–CNT/G nanocomposite were characterized by X-ray diffraction (XRD) using a diffractometer (Rigaku, Cu Kα radiation). The diffraction patterns were recorded in the 2θ range from 10° to 70°. Thermogravimetric analysis (TGA) was conducted on a Pyris 1 TGA (Perkin Elmer, USA) at a heating rate of 10 °C min^{-1} in air from 25 to 800 °C. Tensile tests were performed using an Instron 5848 microtester with a strain rate of 1% per min and a 1 cm gauge length. The microstructures of the S–CNT and S–CNT/G nanocomposite electrodes were characterized using a scanning electron microscope (Sirion 200, FEI) and a transmission electron microscope (Tecnai G2F20, FEI).

Electrochemical measurement

Coin-type half-cells were assembled in a glove box filled with protective argon gas (M. Braun inert gas systems Co. Ltd., Germany) with the S–CNT or S–CNT/G nanocomposite as the working electrode and pure lithium foil as the reference electrode. A polypropylene film (Celgard 2400) was used to separate the cathode and the anode. 1 M LiTFSI solution in ethylene carbonate (DOL) and diethyl carbonate (DME) mixed at a volume ratio of 1 : 1 with 0.2 M $LiNO_3$ as an additive was used as the electrolyte. The discharge and charge measurements were conducted on a Land battery test system (Wuhan Land Electronic Co., China) in a voltage window of 1.9–2.6 V at different charge–discharge rates at room temperature. The rate test was performed by charging the electrode at various charge rates while discharging at a constant rate of 0.5 C. Cyclic voltammetry tests were performed between 1.9 V and 2.6 V at 1 C using a Potentiostat/Galvanostat (EG&G Princeton Applied Research 273A). CV curves before cycling, after the 10th cycle, and after the 50th cycle were tested in sequence.

Results and discussion

The S–CNT/G nanocomposite was synthesized *via* a facile ultrasonication-assisted method (Fig. 1). Sulfur particles,

graphene, and SACNTs were uniformly suspended in a water–ethanol mixed solution *via* intensive ultrasonication. In the suspension, the large surface area of 1D SACNTs and 2D graphene offers abundant adsorption points that allow uniform deposition of sulfur particles. Meanwhile, sulfur particles suppress the re-stacking of graphene and the bundling of SACNTs that ensure a well-distributed 3D conductive porous framework. This homogenous and porous 3D architecture of sulfur, SACNTs, and graphene can be reserved in the suspension after the removal of the solvent, leading to a binder-free composite film with high porosity, conductivity, and flexibility (Fig. S1a†).

It should be mentioned that the ability to form a self-sustained composite film is highly relevant to the CNT/G ratio in the framework. When graphene is added to an amount smaller than or equivalent to that of SACNTs, *i.e.*, for composites with a CNT/G ratio of 1 : 1 and 2 : 1, sufficient SACNTs in the composite work well to form a homogenous and self-sustained composite film with uniform thickness. When the amount of graphene is further increased to a majority in the composite, *i.e.* for composite with a CNT/G ratio of 1 : 2, an insufficient number of SACNTs in the framework deteriorates the ability to form a self-sustained composite film, resulting in a relatively inhomogeneous film with wide divergence in thickness. Fig. S1b† shows the thickness of the S–CNT and S–CNT/G composites, in which the largest diversity can be found in the S–CNT/G composite with a CNT/G ratio of 1 : 2. Under extreme conditions, when there is no SACNT in the composite, graphene tends to aggregate seriously, resulting in many discrete and small pieces at the bottom of the container instead of a continuous film.

A detailed microstructure of the S–CNT/G composite with a CNT/G ratio of 1 : 1 can be revealed by TEM. As shown in Fig. 2a, SACNTs and graphene sheets interweave with each other to form a 3D conductive framework, while at the same time maintaining their individual 1D and 2D characteristics (Fig. S1c and S1d†). In the 3D architecture, SACNTs with 1D structure act as skeleton, while 2D graphene sheets extending across the whole structures provide additional supplement in the other dimension to build the integrated conductive framework and to immobilize sulfur particles. The surface of graphene is rough and crumpled with abundant wrinkles (as marked by the red arrows in Fig. 2a), which may act as buffers to accommodate the volume variation of sulfur when transferring to Li_2S/Li_2S_2. The red arrows in Fig. 2b guide the edge of one graphene sheet, indicating that two graphene sheets marked as "graphene 1" and "graphene 2" in the image overlapped with each other. Sulfur particles tend to uniformly anchor along SACNTs or onto the graphene surface, which ensures that each sulfur particle can be well connected to the conductive framework during the insertion and extraction of lithium. The high-resolution image shown in Fig. 2c elucidates the structural features of one sulfur particle anchored on the graphene surface. The lattice fringes of 3.44 nm correspond to S (026) planes, which reflect the well-defined crystalline structure of sulfur. Based on TEM images of the S–CNT/G composite, a statistical analysis of the particle size distribution reveals that the sulfur particles within the CNT/G framework mostly possess a diameter of 5–20 nm, and over half of the particles show a diameter of 5–15 nm (Fig. 2d). Note that large aggregates are shown in both SEM (Fig. S1e†) and TEM (Fig. S1f†) images of the raw sulfur powder, and each sulfur aggregate consists of a number of small particles of 5–20 nm (Fig. S1f†). The ultrasonic treatment in the synthesis process disperses the individual small particles in the CNT/G framework. During the following process to remove the solvent, the interlinked CNT/G framework prevents the dispersed sulfur particles from reuniting into large aggregates by offering well-dispersed physical barriers among them. No obvious agglomeration of sulfur particles is found in the S–CNT/G composite, revealing the efficiency of the interlinked CNT/G conductive framework in preventing sulfur aggregation. Therefore, well-dispersed active sulfur particles with enhanced electrical contact with CNT/G can be achieved. As a contrast, when there is no CNT/G framework in the solution, large sulfur aggregates of around 50 nm are obtained (Fig. S1f†). When there are only CNTs in the framework, *i.e.* in the S–CNT composite, large sulfur aggregates and bundled CNTs are present (Fig. S1g†). Fig. 2e presents the XRD patterns of pure graphene, SACNTs, and the S–CNT/G composites with various CNT/G ratios. Characteristic peaks of orthorhombic sulfur (marked by the orange column lines according to PDF#08-0247) can be detected in the S–CNT/G composites, suggesting the well crystallized feature of the sulfur particles. Two broad peaks at 26.0° and 22.2°, which correspond to the (002) peaks of SACNTs and graphene respectively, are present in the S–CNT/G composites, showing different intensities considering various CNT/G ratios. The clear peaks of graphene, SACNTs, and sulfur in the composites indicate that sulfur particles anchor uniformly among the 3D homogenous framework of SACNTs and graphene.

The morphologies of the S–CNT/G composites were investigated by SEM. Fig. 3a–c show the SEM images of the surface morphology of the S–CNT/G composites with CNT/G ratios of 2 : 1, 1 : 1, and 1 : 2. In comparison with the bundled structure

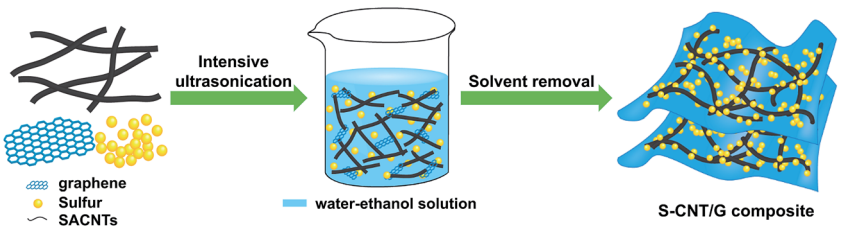

Fig. 1 Schematic of the synthesis procedure of the S–CNT/G composite.

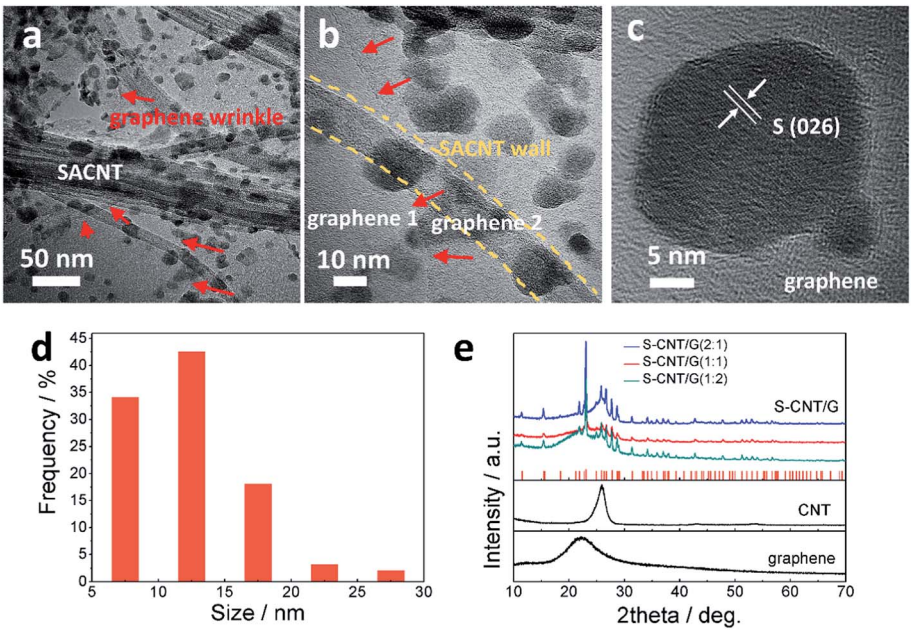

Fig. 2 TEM images of (a and b) the S–CNT/G composite. (c) HRTEM image of one sulfur particle on graphene. (d) Statistical analysis of particle size distribution of sulfur. (e) XRD patterns of the S–CNT/G composites, CNT, and graphene.

in the S–CNT composite (Fig. S1h†), SACNTs and graphene intertwine with each other to form a web structure in the S–CNT/G composites. Note that the surface morphology is highly relevant to the CNT/G ratio in the framework. When graphene is added to a minority (CNT/G = 2 : 1) in the CNT/G framework, SACNTs cannot be fully covered by graphene sheets, with many SACNT bundles visible on the surface (Fig. 3a). On the surface of the composite with a CNT/G ratio of 1 : 1, a flexible thin film of graphene can be found (Fig. 3b). The sample surface is well enfolded by graphene, which can serve as a block layer to restrain sulfur, polysulfides, and their lithiation products (Li_2S/Li_2S_2). EDX elemental analysis in the inset of Fig. 3b shows that elemental sulfur is well distributed across the composite. The surface image of the composite with a CNT/G ratio of 1 : 1 at higher magnification is given in Fig. 3d, in which bundles of SACNTs can be clearly observed through the surface pores. When graphene is added to a majority (CNT/G = 1 : 2), the excess graphene sheets tend to produce wrinkles across the surface (Fig. 3c). In all the three samples, no large sulfur aggregates can be found by SEM, suggesting that sulfur is uniformly embedded in the CNT/G structures to form an inseparable complex. The interior and cross-sectional morphologies of the composite were further examined. The S–CNT/G composites with various CNT/G ratios give similar

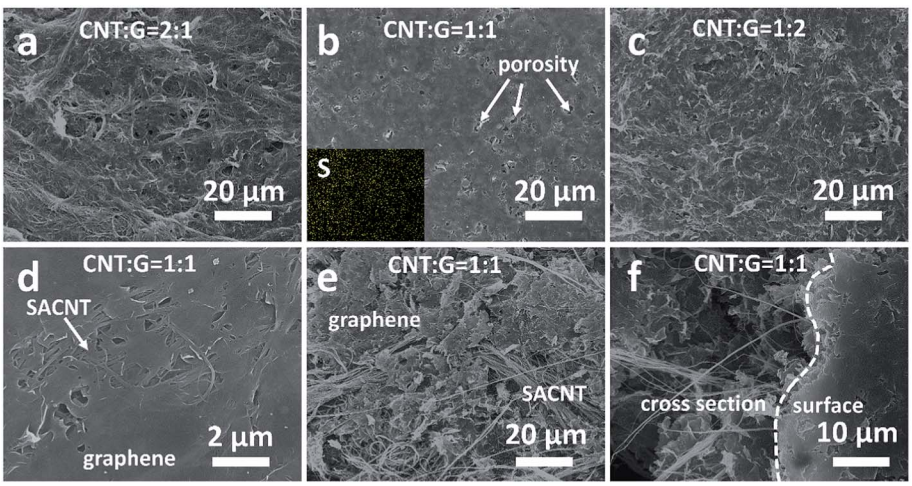

Fig. 3 SEM images of the surface morphology of the S–CNT/G composites with CNT/G ratios of (a) 2 : 1, (b) 1 : 1, (c) 1 : 2, and (d) 1 : 1 at higher magnification. The inset of (b) gives the EDX elemental analysis of sulfur. (e and f) show the interior and cross-sectional morphology of the S–CNT/G composite with a CNT/G ratio of 1 : 1, respectively.

morphologies, and the typical images of the S–CNT/G composite with a CNT/G ratio of 1 : 1 are given in Fig. 3e and 3f. The interior morphology in Fig. 3e indicates that SACNTs and graphene are uniformly distributed in the interior structures with abundant porosity. The cross-sectional image in Fig. 3f demonstrates the uniform distribution of SACNTs and graphene along the thickness direction of the composite. Similarly, no large sulfur particles can be found, revealing the efficiency of the CNT/G framework to localize sulfur and prevent its aggregation.

Stress–strain curves of the S–CNT and S–CNT/G composites are shown in Fig. 4a. The S–CNT composite presents a strength of 0.62 MPa and a Young's modulus of 36.14 MPa. In the S–CNT/G composites, the introduced 2D graphene sheets intertwine with or twist around the CNT bundles, resulting in the mechanical reinforcement of the CNT/G hybrid framework. For the composite with a CNT/G ratio of 2 : 1, the strength and the Young's modulus increase to 1.41 MPa and 50.46 MPa, respectively. The largest strength and Young's modulus are obtained in the composite with a CNT/G ratio of 1 : 1, which possesses 345% of the strength (2.14 MPa) and 187% of the Young's modulus (67.55 MPa) of the S–CNT composite. A further increase of graphene content to the CNT/G ratio of 1 : 2 leads to a dramatic decrease in both the strength and Young's modulus to 1.41 MPa and 50.46 MPa, respectively, which is possibly due to the inhomogeneity of the composite film with insufficient SACNT skeleton in the framework. For the S–CNT/G composite with a CNT/G ratio of 1 : 1, the strain at fracture is 4.96%, which is 132% of the one in the S–CNT composite (3.75%). Both the high strength and high flexibility are beneficial for enduring the volume changes of the sulfur electrode during cycling and achieving better cycling stability.

TGA results of graphene, S–CNT, and S–CNT/G composites are given in Fig. 4b. Pure graphene exhibits a one-step weight loss in the temperature range of 400–600 °C, and the S–CNT composite presents a two-step weight loss at around 150–300 °C and 500–740 °C corresponding to the evaporation of sulfur and decomposition of SACNTs. Consequently, a three-step weight loss is observed in the S–CNT/G composite corresponding to the loss of sulfur, graphene, and SACNTs, respectively. The weight percentages of sulfur in both the S–CNT and S–CNT/G composites are around 50%, consistent with that designed in the raw materials. The curves within the grey square are enlarged in the inset of Fig. 4b. Compared to the S–CNT composite, composites with increased graphene content, *i.e.* the S–CNT/G composites with CNT/G ratios of 2 : 1 and 1 : 1, show an elevated sulfur loss temperature, which is due to the retarding effect of graphene when sulfur is escaping from the composite. As graphene content increases further, *i.e.* in the S–CNT/G composite with a CNT/G ratio of 1 : 2, an insufficient number of SACNTs causes difficulty in forming a self-sustained film and weakens the physical restrain to the sulfur particles, resulting in a slightly lower sulfur loss temperature than that in the S–CNT/G composite with a CNT/G ratio of 1 : 1. The decomposition temperatures of graphene and SACNTs overlap, therefore it is hard to determine their exact weight percentages through the TGA curves. But as there is almost no weight loss in the synthesis process, the CNT/G ratios in the S–CNT/G composites are considered to be the same with that in the raw materials.

In order to demonstrate the structural benefits of CNT/G hybrids for improving the performance of the sulfur electrode, coin-type half-cells of the S–CNT/G composites against the lithium metal counter electrode were assembled to conduct the galvanostatic charge–discharge measurement. The S–CNT and S–CNT/G composites were cycled at various charge rates while being discharged at a constant rate of 0.5 C in the voltage window between 1.9 and 2.6 V. Fig. 5a presents the rate capability of the S–CNT and S–CNT/G composites with various graphene contents, among which the composite with an equivalent amount of SACNTs and graphene (CNT/G = 1 : 1) possesses the largest capacities. A discharge capacity of 1172–1147 mA h g^{-1} is obtained at the rate of 0.5 C in 6 cycles, and these values are 1123–1121, 1078–1070, and 1012–987 mA h g^{-1} in subsequent cycles at 1 C, 2 C, and 5 C, respectively. At a rate of 10 C, the specific discharge capacity is as high as 938–920 mA h g^{-1}, delivering appealing high-rate performance. When the high-rate cycled battery was consequently cycled at smaller rates of 0.5 C and 0.2 C, large capacities of 1012–1000 and 1035–995 mA h g^{-1} can still be obtained again, demonstrating its excellent reversibility. Apart from the composite with a CNT/G ratio of 1 : 1, the composite with minor addition of graphene

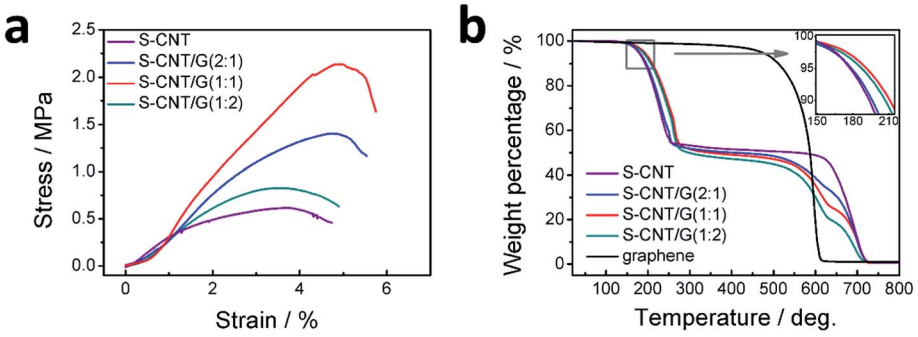

Fig. 4 (a) Stress–strain curves of the S–CNT and S–CNT/G composites. (b) TGA results of graphene, the S–CNT composite, and the S–CNT/G composites. The inset of (b) gives the enlarged view of the square in (b).

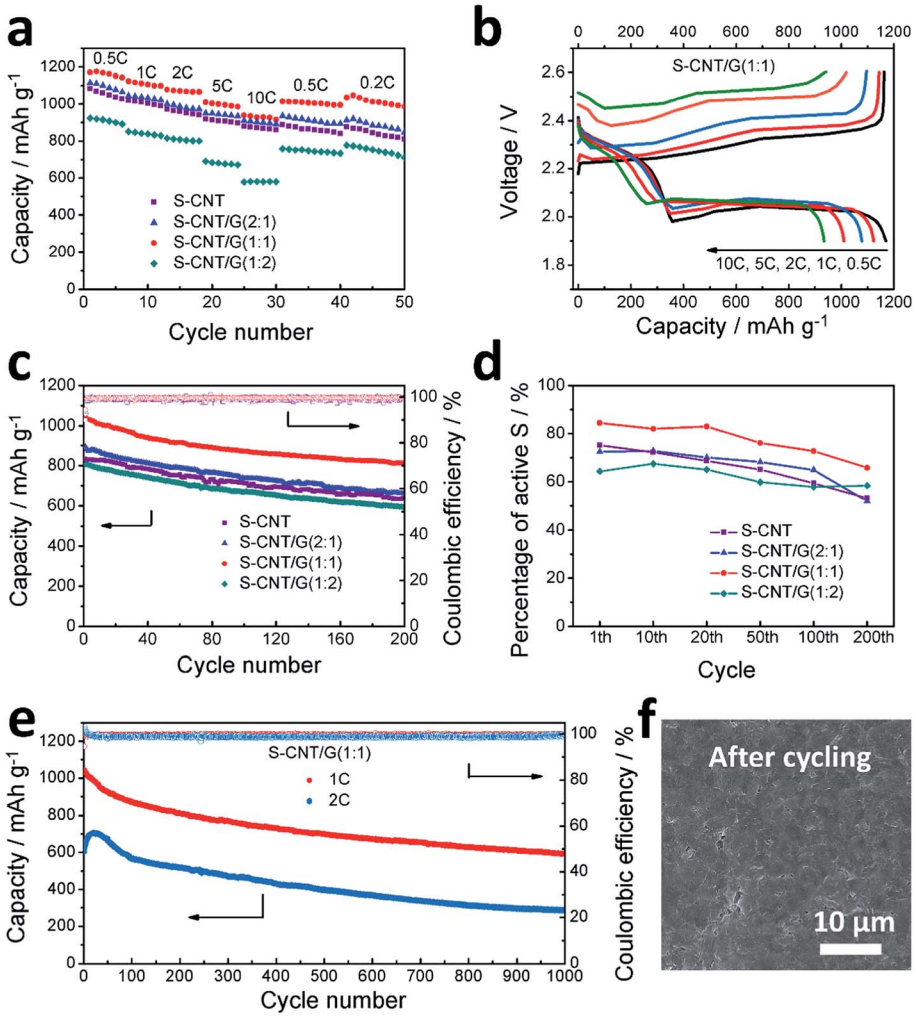

Fig. 5 (a) Rate performance, (b) galvanostatic charge–discharge curves, (c) cycle performance at 1 C, (d) percentage of active sulfur with increased cycle numbers at 1 C of the S–CNT and S–CNT/G composites. (e) Long term cycling behavior of the S–CNT/G composite with a CNT/G ratio of 1 : 1 at 1 C and 2 C. (f) SEM image of the S–CNT/G composite with a CNT/G ratio of 1 : 1 after cycling.

(CNT/G = 2 : 1) also shows acceptable capacities, *i.e.* 1121–1067 mA h g^{-1} at 0.5 C, 1045–1064 mA h g^{-1} at 1 C, 1011–973 mA h g^{-1} at 2 C, 952–940 mA h g^{-1} at 5 C, and 905–889 mA h g^{-1} at 10 C, superior to the S–CNT composite with only the 1D CNT conductive component. Based on the microstructure morphology and mechanical behavior discussed above, the increased capacities in the composite with CNT/G ratios of 1 : 1 are understandable. The addition of graphene in the SACNT skeleton provides additional 2D confinement to localize sulfur particles and ensures a well-connected conductive framework for sulfur particles, which shortens the electron transfer pathway and leads to superior high-rate performance. However, excessive addition of graphene will lead to a relatively inhomogeneous film and deteriorate the mechanical performance of the composite, resulting in unsatisfactory electrochemical performance. In fact, when graphene is added to a CNT/G ratio of 1 : 2, the amount of SACNTs in the composite becomes too small to form a homogeneous framework, which accounts for its lowest rate performance.

The 1st cycle discharge and charge voltage profiles of the S–CNT/G composite with a CNT/G ratio of 1 : 1 at various current rates from 0.5 C to 10 C are shown in Fig. 5b. The discharge curves present the same pattern, with typical two-plateau behavior corresponding to the formation of polysulfides (Li_2S_n, n = 4–7) at 2.3 V and short-chain Li_2S_2/Li_2S at 2.1 V, in agreement with the cyclic voltammetry (CV) test that presents two main reduction peaks (Fig. S2a†). The second plateau is very flat, indicating a uniform deposition of Li_2S with little kinetic barriers. Furthermore, the plateau corresponding to the generation of polysulfides remains constant and high, indicating the efficiency of the composite in trapping polysulfides. Steady discharge behavior and large capacity are present even at high charge rates. For example, at the charge rate of 10 C (6 minutes to finish full charge of the cathode), the composite can still exhibit 80% of the discharge capacity at 0.5 C. The excellent electrochemical behavior at high charge rates is of great value for practical applications of lithium–sulfur batteries.

Apart from the excellent rate performance, the S–CNT/G nanocomposite also exhibits favorable cycling behavior at 1 C (Fig. 5c). Similar to the rate tests, the S–CNT/G composites with CNT/G ratios of 2 : 1 and 1 : 1 exhibited superior cycling performance compared to the S–CNT composite. Optimal performance is also obtained in the composite with a CNT/G ratio of 1 : 1, which delivers an initial capacity of 1048 mA h g^{-1} and a final capacity of 818 mA h g^{-1} in 200 cycles, corresponding to a capacity retention of 78%. As the sulfur particles in the electrode need to contact the electrolyte for efficient lithium ion transfer, dissolution of polysulfides into the electrolyte and consequent loss of active sulfur cannot be thoroughly avoided, which accounts for the small capacity decay of 0.11% per cycle during the cycling process. Both the positions and areas of the CV peaks of the S–CNT/G composite (Fig. S2a†) remain almost unchanged before cycling, after the 10th cycle, and after the 50th cycle, suggesting its high electrochemical stability, which is consistent with good capacity retention. These results are also in agreement with the charge–discharge profiles, where two clear plateaus indicate stable lithium insertion/extraction behavior in the 1st cycle and subsequent 200 cycles (Fig. S2b†). Apart from the composite with a CNT/G ratio of 1 : 1, acceptable capacities are also obtained in the composite with a CNT/G ratio of 2 : 1 that possesses discharge capacities of 898–664 mA h g^{-1} in 200 cycles. In comparison, the S–CNT and S–CNT/G composite with a CNT/G ratio of 1 : 2 can only deliver capacities of 810–595 and 805–597 mA h g^{-1} respectively in 200 cycles. The average coulombic efficiencies in all the samples are above 99%, demonstrating the efficiency of the CNT/G based 3D conductive framework in retarding the shuttle of polysulfides. Capacities vary in the S–CNT/G composites with different CNT/G ratios, declaring various efficiencies of SACNT and graphene in increasing sulfur utilization and promoting deep lithiation. Such an effect can be confirmed by the analysis of the charge–discharge curves. Generally, the first plateau in the charge–discharge curve corresponding to the transfer from elemental sulfur (S_8) to polysulfides indicates the utilization of the active material, *i.e.*, percentage of active sulfur, and the second plateau corresponding to the transfer from polysulfides to Li_2S/Li_2S_2 indicates the deep lithiation degree of sulfur, *i.e.*, x in the final lithiation product Li_xS.[28] By carefully examining the capacity contribution from the two plateaus, both percentage of active sulfur and lithiation degree of sulfur can be revealed. Fig. 5d shows the percentage of active sulfur in the S–CNT/G composites as a function of the cycle numbers. Consistent with the cycling performance given in Fig. 5c, the S–CNT/G composite with a CNT/G ratio of 1 : 1 exhibits the largest sulfur utilization throughout the 200 cycles, with the percentage of active sulfur being 84%, 82%, 83%, 75%, 73%, and 66% in the 1st, 10th, 20th, 50th, 100th, and 200th cycle, respectively. Moreover, deepest lithiation is also obtained in the S–CNT/G composite with a CNT/G ratio of 1 : 1, with a stable lithiation degree of around 1.2 in the 200 cycles (Fig. S2d†). The increased sulfur utilization and lithiation degree are ascribed to the properly introduced graphene in the SACNT framework. Compared to pure SACNTs, the CNT/G hybrids provide more adsorption points to localize sulfur and polysulfides, prevent aggregation of the active material and its lithiation products, and consequently increase the sulfur utilization and promote deep lithiation of sulfur. At the same time, the introduced graphene, along with the ultrasonication-assisted synthesis process, also prevents bundling of SACNTs, ensures a well-distributed 3D conductive porous framework of SACNTs and graphene, and yields a synergetic effect among SACNTs, graphene, and sulfur.

An extremely long-term cycling test was also conducted for the S–CNT/G composite with a CNT/G ratio of 1 : 1 at 1 C. A high final discharge capacity of 594 mA h g^{-1} is obtained after 1000 cycles, corresponding to a capacity fade as small as 0.041% per cycle (Fig. 5e). Even when the cycling rate is increased to 2 C, the composite can still exhibit an initial capacity of 600 mA h g^{-1}, a final capacity of 293 mA h g^{-1} after 1000 cycles and a capacity fade of 0.054% per cycle. Besides, the coulombic efficiency remains above 99% over long term cycling, indicating the alleviation of the shuttle effect. As a contrast, the S–CNT composite presents a large capacity drop to 339 mA h g^{-1} after 1000 charge–discharge cycles (Fig. S2d†). The long-term cycling performance of the S–CNT/G composite is among the best results reported so far on sulfur cathodes.[16,34,35] For example, Liu and co-workers wrapped graphene over sulfur-coated carbon nanofibers and obtained a capacity smaller than 400 mA h g^{-1} after 1000 cycles at 1 C.[34] Cui and co-workers designed a sulfur–TiO_2 yolk–shell nanoarchitecture and demonstrated a capacity around 700 mA h g^{-1} at a smaller cycling rate of 0.5 C.[35] Zhang and co-workers employed a cetyltrimethyl ammonium bromide (CTAB)-modified sulfur–graphene oxide (S–GO) nanocomposite cathode and achieved a capacity around 500 mA h g^{-1} at 1 C.[16] The superior long-term cycling performance of the S–CNT/G composite further confirms the great advantage of the 3D CNT/G hybrid structure. After cycling, the morphology of the composite with a CNT/G ratio of 1 : 1 was examined. As shown in Fig. 5f, no mechanical crack or large agglomerate of insulating Li_2S/Li_2S_2 can be found on the surface of the electrode, indicating that the CNT/G hybrid framework with abundant adsorption points and physical barriers effectively prevents agglomeration of the electrode material and provides physical confinement to sulfur/polysulfides to ensure enhanced electrochemical performance of the electrode.

Compared to other S–CNT/G hybrid materials with complex structures reported in literature, the 3D CNT/G hybrid conductive framework with much porosity promises a short and rapid charge transfer pathway, efficient electrolyte infiltration, and multi-dimensional restrain to trap sulfur and polysulfides. Large interior space is also provided to accommodate the significant volume changes for sulfur during cycling and a large conductive surface area for depositing insulating Li_2S_2 and Li_2S, in order to preserve the morphology of the electrodes. All these characteristics mentioned above account for the excellent cycling and high rate performances of the S–CNT/G composite. Besides, properly introduced graphene also increases the mechanical strength and flexibility of the electrode, which is of great value in flexible batteries. Moreover, compared to other methods to produce the S–CNT/G composite, such as thermal evaporation, infiltration, or solution reaction, the

ultrasonication-assisted synthesis process of the S–CNT/G composite is simple and energy-efficient.

Conclusions

In summary, we have successfully prepared S–CNT/G composites *via* a simple ultrasonication-assisted method. In this architecture, 1D SACNTs combine with 2D graphene to form a 3D hybrid conductive framework to host sulfur nanoparticles. The composite with an optimal CNT/G ratio of 1 : 1 exhibits a specific capacity up to 1172 mA h g^{-1} at 0.5 C and impressive rate capabilities with a capacity of 938 mA h g^{-1} at a charge rate as high as 10 C. Remarkably, a high capacity of 594 mA h g^{-1} after 1000 cycles at 1 C is achieved, which belongs to one of the best results reported so far on sulfur cathodes. These results clearly demonstrate the advantage of the unique 1D SACNT/2D graphene hybrid framework in constructing sulfur composite structures for high performance lithium sulfur batteries.

Acknowledgements

This work was supported by the National Basic Research Program of China (2012CB932301), NSFC (51102146 and 51472141), and the NCET Program of China.

Notes and references

1 L. Chen and L. L. Shaw, *J. Power Sources*, 2014, **267**, 770–783.
2 G. Y. Xu, B. Ding, J. Pan, P. Nie, L. F. Shen and X. G. Zhang, *J. Mater. Chem. A*, 2014, **2**, 12662–12676.
3 Y. X. Yin, S. Xin, Y. G. Guo and L. J. Wan, *Angew. Chem., Int. Ed.*, 2013, **52**, 13186–13200.
4 D. W. Wang, Q. C. Zeng, G. M. Zhou, L. C. Yin, F. Li, H. M. Cheng, I. R. Gentle and G. Q. M. Lu, *J. Mater. Chem. A*, 2013, **1**, 9382–9394.
5 Y. S. Su, Y. Z. Fu and A. Manthiram, *Phys. Chem. Chem. Phys.*, 2012, **14**, 14495–14499.
6 J. C. Guo, Y. H. Xu and C. S. Wang, *Nano Lett.*, 2011, **11**, 4288–4294.
7 S. C. Han, M. S. Song, H. Lee, H. S. Kim, H. J. Ahn and J. Y. Lee, *J. Electrochem. Soc.*, 2003, **150**, A889–A893.
8 L. X. Yuan, H. P. Yuan, X. P. Qiu, L. Q. Chen and W. T. Zhu, *J. Power Sources*, 2009, **189**, 1141–1146.
9 W. Weng, V. G. Pol and K. Amine, *Adv. Mater.*, 2013, **25**, 1608–1615.
10 K. K. Jin, X. F. Zhou, L. Z. Zhang, X. Xin, G. H. Wan and Z. P. Liu, *J. Phys. Chem. C*, 2013, **117**, 21112–21119.
11 L. W. Ji, M. M. Rao, H. M. Zheng, L. Zhang, Y. C. Li, W. H. Duan, J. H. Guo, E. J. Cairns and Y. G. Zhang, *J. Am. Chem. Soc.*, 2011, **133**, 18522–18525.
12 S. Evers and L. F. Nazar, *Chem. Commun.*, 2012, **48**, 1233–1235.
13 J. Z. Wang, L. Lu, M. Choucair, J. A. Stride, X. Xu and H. K. Liu, *J. Power Sources*, 2011, **196**, 7030–7034.
14 Y. L. Cao, X. L. Li, I. A. Aksay, J. Lemmon, Z. M. Nie, Z. G. Yang and J. Liu, *Phys. Chem. Chem. Phys.*, 2011, **13**, 7660–7665.
15 G. M. Zhou, S. F. Pei, L. Li, D. W. Wang, S. G. Wang, K. Huang, L. C. Yin, F. Li and H. M. Cheng, *Adv. Mater.*, 2014, **26**, 625–631.
16 M. K. Song, Y. G. Zhang and E. J. Cairns, *Nano Lett.*, 2013, **13**, 5891–5899.
17 J. P. Rong, M. Y. Ge, X. Fang and C. W. Zhou, *Nano Lett.*, 2014, **14**, 473–479.
18 J. L. Wang, J. Yang, J. Y. Xie, N. X. Xu and Y. Li, *Electrochem. Commun.*, 2002, **4**, 499–502.
19 X. L. Ji, K. T. Lee and L. F. Nazar, *Nat. Mater.*, 2009, **8**, 500–506.
20 B. Zhang, X. Qin, G. R. Li and X. P. Gao, *Energy Environ. Sci.*, 2010, **3**, 1531–1537.
21 S. C. Wei, H. Zhang, Y. Q. Huang, W. K. Wang, Y. Z. Xia and Z. B. Yu, *Energy Environ. Sci.*, 2011, **4**, 736–740.
22 J. X. Song, T. Xu, M. L. Gordin, P. Y. Zhu, D. P. Lv, Y. B. Jiang, Y. S. Chen, Y. H. Duan and D. H. Wang, *Adv. Funct. Mater.*, 2014, **24**, 1243–1250.
23 Z. Li, L. X. Yuan, Z. Q. Yi, Y. M. Sun, Y. Liu, Y. Jiang, Y. Shen, Y. Xin, Z. L. Zhang and Y. H. Huang, *Adv. Energy Mater.*, 2014, **4**, 1301473.
24 J. W. Kim, J. D. Ocon, D. W. Park and J. Lee, *ChemSusChem*, 2014, **7**, 1265–1273.
25 C. H. Xu, B. H. Xu, Y. Gu, Z. G. Xiong, J. Sun and X. S. Zhao, *Energy Environ. Sci.*, 2013, **6**, 1388–1414.
26 X. F. Li, J. L. Yang, Y. H. Hu, J. J. Wang, Y. L. Li, M. Cai, R. Y. Li and X. L. Sun, *J. Mater. Chem.*, 2012, **22**, 18847–18853.
27 X. F. Li and C. L. Wang, *J. Mater. Chem. A*, 2013, **1**, 165–182.
28 C. Tang, Q. Zhang, M. Q. Zhao, J. Q. Huang, X. B. Cheng, G. L. Tian, H. J. Peng and F. Wei, *Adv. Mater.*, 2014, **26**, 6100–6105.
29 M. Q. Zhao, X. F. Liu, Q. Zhang, G. L. Tian, J. Q. Huang, W. C. Zhu and F. Wei, *ACS Nano*, 2012, **6**, 10759–10769.
30 J. Xie, J. Yang, X. Y. Zhou, Y. L. Zou, J. J. Tang, S. C. Wang and F. Chen, *J. Power Sources*, 2014, **253**, 55–63.
31 K. L. Jiang, Q. Q. Li and S. S. Fan, *Nature*, 2002, **419**, 801.
32 K. L. Jiang, J. P. Wang, Q. Q. Li, L. A. Liu, C. H. Liu and S. S. Fan, *Adv. Mater.*, 2011, **23**, 1154–1161.
33 L. Sun, M. Y. Li, Y. Jiang, W. B. Kong, K. L. Jiang, J. P. Wang and S. S. Fan, *Nano Lett.*, 2014, **14**, 4044–4049.
34 S. T. Lu, Y. W. Cheng, X. H. Wu and J. Liu, *Nano Lett.*, 2013, **13**, 2485–2489.
35 Z. W. Seh, W. Y. Li, J. J. Cha, G. Y. Zheng, Y. Yang, M. T. McDowell, P. C. Hsu and Y. Cui, *Nat. Commun.*, 2013, **4**, 1331.

